Solid Freeform Fabrication 2023: Proceedings of the 34th Annual International Solid Freeform Fabrication Symposium – An Additive Manufacturing Conference
Reviewed Paper

Effect of Printing Parameters on the Internal Geometry of Products Manufactured by Fused Filament Fabrication (FFF)

Benjamín A. Moreno-Núñez[†, *], Cecilia D. Treviño-Quintanilla[♦, *], Juan Carlos Espinoza-García[†], Esmeralda Uribe-Lam[†] and Enrique Cuan-Urquizo[♦].

[†]School of Engineering and Sciences, Tecnologico de Monterrey, QRO 76130
[♦]Institute of Advanced Materials for Sustainable Manufacturing, Tecnologico de Monterrey, QRO 76130
[*]Corresponding authors

Abstract

The internal geometry of a 3D-printed product determines its mechanical properties. In Fused Filament Fabrication (FFF) the filaments that build up the internal geometry suffer from variations that have not been sufficiently studied. This research focused on identifying the parameters that most affect the filaments and finding the optimum values to reduce their variations. A fractional factorial design of experiments was used to detect the printing parameters of FFF that most affect the width of extruded filaments, these results were also statistically analyzed. A response optimization was done to obtain the values of the printing parameters that will give the closest width of extruded filaments to the nozzle of the 3D printer used. Results showed layer height has the largest impact on filament width variation.

Keywords: additive manufacturing, fused filament fabrication, statistical analysis, fractional factorial design, internal geometry, thermoplastics.

Introduction

A modern manufacturing technique used to create structural, athletics, medical, and aeronautical devices is additive manufacturing (AM) [1–4]. AM can contribute to reduce production costs in low-volume lines or industries involved in new product development [2]. A process that is part of AM processes is Fused Filament Fabrication (FFF), also called Fused Deposition Modelling (FDM), a technology first developed by Stratasys® [5] to accomplish 3D-printed products. The FFF process consists in heating up and extruding a thermoplastic filament through a nozzle that deposits it on specific zones and uses a layer-by-layer method upon finishing the desired geometry.

During the FFF process, the G-code is the primary component and is in charge of modifying the printing parameters [6–8]. Some of the printing parameters that G-code can control are nozzle movement, extrusion temperature, feed rate, bed temperature, printing speed, fan, or layer thickness [9]. The printing parameters have a direct effect in the thermoplastics used in FFF, they can create defects, like weak bonding or porosity [10] on the structure due to the interaction of mechanical operation and thermal changes [11,12]. These structural defects will impact the mechanical response, diminishing mechanical properties on products made with thermoplastic filaments [11,13–17].

The dimensional accuracy of FFF products is a critical point for the mechanical response of the FFF products, this accuracy can be affected by the printing parameter variations. The FFF products have lower dimensional accuracy (2.2% of volumetric variation) when compared to

foamed or injected thermoplastic products (1.3% of volumetric variation) [18]. Dimensional accuracy can be affected by infill density, extrusion rate, feed rate, nozzle diameter, the length of the extruder travel, layer accumulation, or by the tangential velocity of the printing path [19–22].

One part of dimensional accuracy is the filament width, which can affect the mechanical response of FFF products because it is related to the infill geometry of them. The infill geometries are included in FFF products to have high strength and a relative low mass [23]. A variation in the infill pattern, layer thickness, or lack of uniformity will cause variating strength, quality, and behavior of FFF products [24,25]. It has been found that the filament can be affected by nozzle speed, the higher the nozzle speed, the smaller the filament diameter [26]. Also, the viscoelastic stresses produced in the 3D-printing process can affect the extruded filament dimensions [27].

Statistics have been used in FFF to analyze physical and mechanical responses, the most common methods used are response surface [28–31], Taguchi methodology [32,33], central composite design [31,34,35], and fractional factorial design [29,36]. These models have been used in the FFF process to make regression models that can help to optimize the printing process parameters and improve the properties of the final 3D-product [20,34,36–39]. Regression analyses like surface methodology, support vector regression, or multivariable linear regression have been used in FFF processes and products to make regression models that predict and optimize flexural properties [30], dynamic mechanical performance [39], tensile strength [40–42], creep rate [43], flexural properties [44], warpage [45,46], or surface roughness [28,47,48]. More modern techniques like artificial neural networks [22] or Gaussian process regression [48] can give more accurate results but require more factors that can be translated to time consumption [22].

Full factorial design has been used to analyze the physical responses of FFF products, for example Vyavahare et al., they used a factorial design to evaluate the effect of five parameters on surface roughness, dimensional accuracy, and time of fabrication on ABS 3D-printed products [28]. Sood et al. used a factorial design to analyze the sliding wear of FFF products, using the response of five parameters adjusted to a factorial design and train an artificial neural network [31]. Santana et al. used a Taguchi L8 orthogonal array and a full factorial design to study the effect of 8 parameters on the dimensional quality of 3D-printed PLA products [20]. Armillotta et al. analyzed the warpage effect of ABS 3D-printed products using 4 printing parameters and a full factorial design [46]. García Plaza et al. used a full factorial design to study 3D-printed PLA geometric properties and the effect on them of 3 printing process parameters, also using the obtained data to feed an artificial neuronal network and make predictions [22].

Some authors have studied the extrusion process and the impact on filament width. Gleadall et al. made a model that simulates the extrusion process of FFF and reached an approximation of filament width with a 5% of error in the 3D-generated-models of engineering scaffolds [49]. Hebda et al. made a model that can predict the filament width, considering the deposition height equal to the nozzle set gap height [50]. Yousefi et al. analyzed the extrudate swell of polycaprolactone (PCL) scaffolds made on a 3D-bioplotter, using an I-optimal, split-plot experiment. In this experiment it has been analyzed the effect of needle diameter, temperature, pressure, and dispensing speed into swell, density, and modulus of the 3D-printed samples. With the results of the experiment, they made 3 regression models for the 3 responses, having percentage differences of 9.5% for swell, 19% for density, and 29% for modulus [51].

The products obtained from FFF suffer from dimensional inaccuracy and do not meet the requirements to be used as functional parts because of the high risk of failure due to variations in

the structure [52]. The aim of this research is to diminish the variation in the width of the individual filaments used to create the infill geometry found inside the products made by FFF, resulting in a homogeneous structure that can make functional 3D-printed products. To achieve this, there were selected the most common FFF printing parameters that can be modified in commercial slicer software, to obtain with their modifications the lower error in their width. Also, this research aims to obtaining the printing parameter values that can reduce the mentioned variation of filament width by obtain regression models that can be set depending on the materials and type of 3D printer used.

Materials and Methods

Materials

The samples were fabricated by FFF, using three different thermoplastic filaments, Polylactic Acid (PLA), Acrylonitrile Butadiene Styrene (ABS), and Polycarbonate (PC). The filaments have a diameter of 1.75 mm and 2.85 mm, provided by Colorplus 3D (Mexico) and XinYuDa (XYD) Plastic Products Factory (China). All filaments were selected white to diminish the dimensional variation caused by the color of the filament [53].

3D Printing Process

To fabricate the samples used in this research, two different printer types were used, a Cartesian printer, Ultimaker 2+ (Netherlands), and a Delta printer, RostockMax V3.2 (USA). The nozzles used to obtain the parts have a diameter of 400 μm, and 500 μm, for Cartesian and Delta printers, respectively. The samples were configured to have 4 alternated layers, 2 with horizontal printing direction and 2 with vertical printing direction, as presented in Figure 1A, to accomplish a 2D square lattice infill geometry. The separation between individual filaments was 1.5 mm, as presented in Figure 1B.

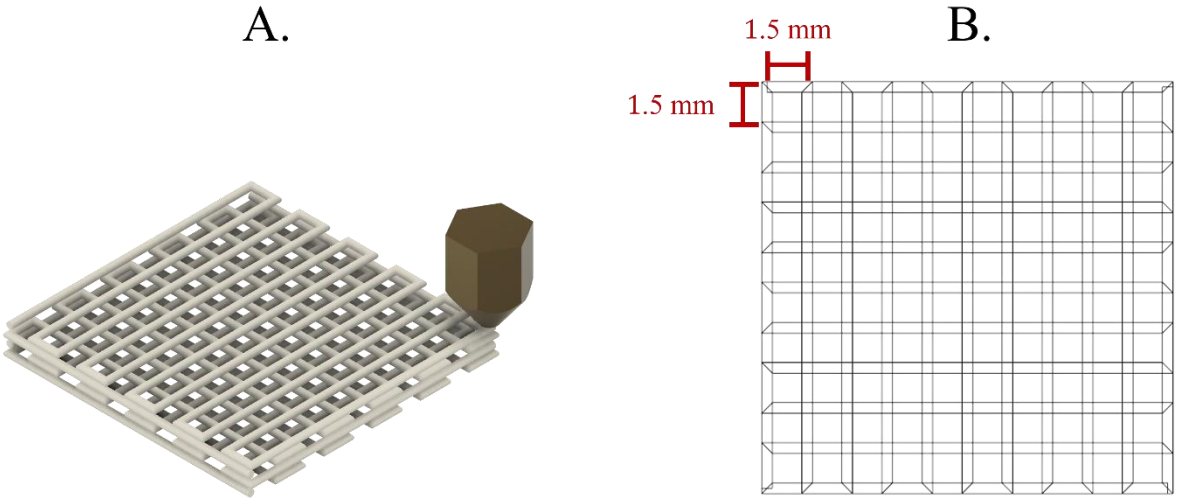

Figure 1. A. Scheme of fabricated samples and B. Separation between individual filaments.

To analyze the effect of the parameters on the extruded filament width, a fractional factorial design of experiments was made for each material and 3D-printer used in this research. Five printing parameters were selected to study their effect on extruded filament width, Extrusion Temperature (ET), Feed Rate (FR), Layer Height (LH), Fan Power (F), and Bed Temperature (BT).

A generic fractional factorial design is displayed in Table 1, where the sign (-) represents the low level and the sign (+) represents the high level of each printing parameter. The samples made for this research followed the runs presented in Table 1. Each printing run was done in the same place of the printing bed with 3 samples printed at a time, repeating this process 3 times, resulting in a total of 144 samples for each printer.

Table 1. Fractional factorial design for FFF process parameters effect on the extruded filament width

Run	*ET*	*FR*	*LH*	*F*	*BT*
1	+	+	+	-	-
2	-	-	+	+	+
3	+	+	+	+	+
4	+	-	-	-	-
5	+	-	+	-	+
6	+	-	+	+	-
7	-	+	+	+	-
8	+	+	-	-	+
9	-	-	+	-	-
10	+	+	-	+	-
11	-	-	-	+	-
12	-	+	-	+	+
13	-	+	+	-	+
14	-	+	-	-	-
15	+	-	-	+	+
16	-	-	-	-	+

The values of the factorial design vary depending on the material and printer used. For ET and BT, the values depend on the material, these are presented in Table 2. For FR, LH, and F, the values depend on the 3D printer and nozzle to be used in the manufacturing process, these are presented in Table 3. These parameters have an impact on the whole printing process and can be configured by the users of 3D printers in any open-source slicer software.

Table 2. High and low-level values for ET and BT parameters for PLA, ABS, and PC filaments.

	PLA		*ABS*		*PC*	
Parameter	*Low*	*High*	*Low*	*High*	*Low*	*High*
ET	200°C	215°C	220°C	250°C	250°C	270°C
BT	50°C	60°C	60°C	80°C	70°C	80°C

Table 3. High and low-level values for FR, LH, and F parameters for Cartesian and Delta printers.

	Cartesian		*Delta*	
Parameter	*Low*	*High*	*Low*	*High*
FR	1440 mm3/s	1800 mm3/s	720 mm3/s	900 mm3/s
LH	0.1 mm	0.2 mm	0.2 mm	0.3 mm
F	OFF (0)	ON (1)	OFF (0)	ON (1)

Optical microscopy

After the printing process, the extruded filament width (W) of the printed samples was characterized using Optical Microscopy (OM). An AXIOCam ICc5 optical microscope, equipped with AxioVision SE64, was used to obtain the image and measurements of W. The top layer of the samples was the one analyzed to obtain the W measurements because it is not flat like the first layer that adheres to the printer bed.

To allow a single filament to be observed under the microscope, it was used a magnification of 50x to analyze the W. 3 measurements were made along the length of the filament, as seen in Figure 2A, to measure the variation of W in the whole infill structure. The units of the measurements given by the microscope software were micrometers [μm], as represented in Figure 2B. The results of the OM were analyzed using MINITAB® as a statistical software program to obtain the regression models and residual analysis presented next.

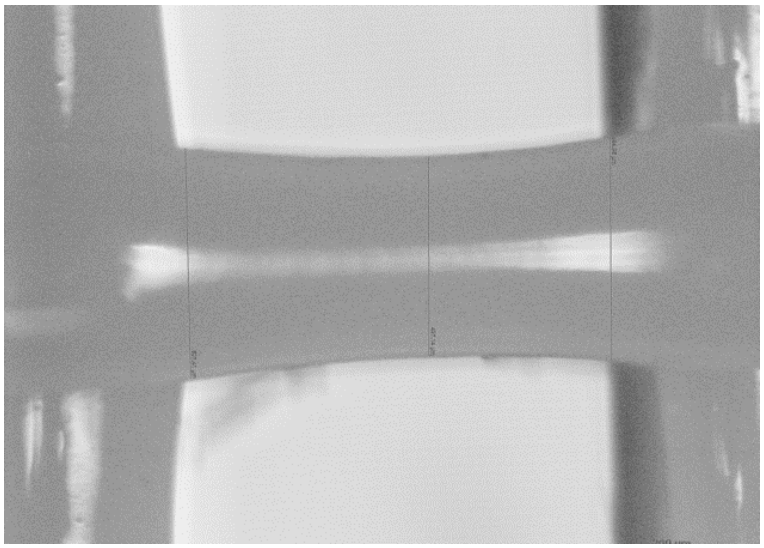

Figure 2. Image of a single filament subjected to OM.

Results and Discussion

The W results from optical microscopy were plotted using the means of the samples measured in each run configuration, these results are presented in Figure 3. Two regression analyses were done to obtain the parameter effects and interactions on W. The first regression was done to detect the parameters and the interactions that have a significant effect on the response. The second regression was done using only the parameters and interactions with significant effects obtained in the first regression. This results in a reduced number of parameters used in the models but maintaining a R^2 higher than 70%, meaning that at least 70% of the process can be described with the parameters used.

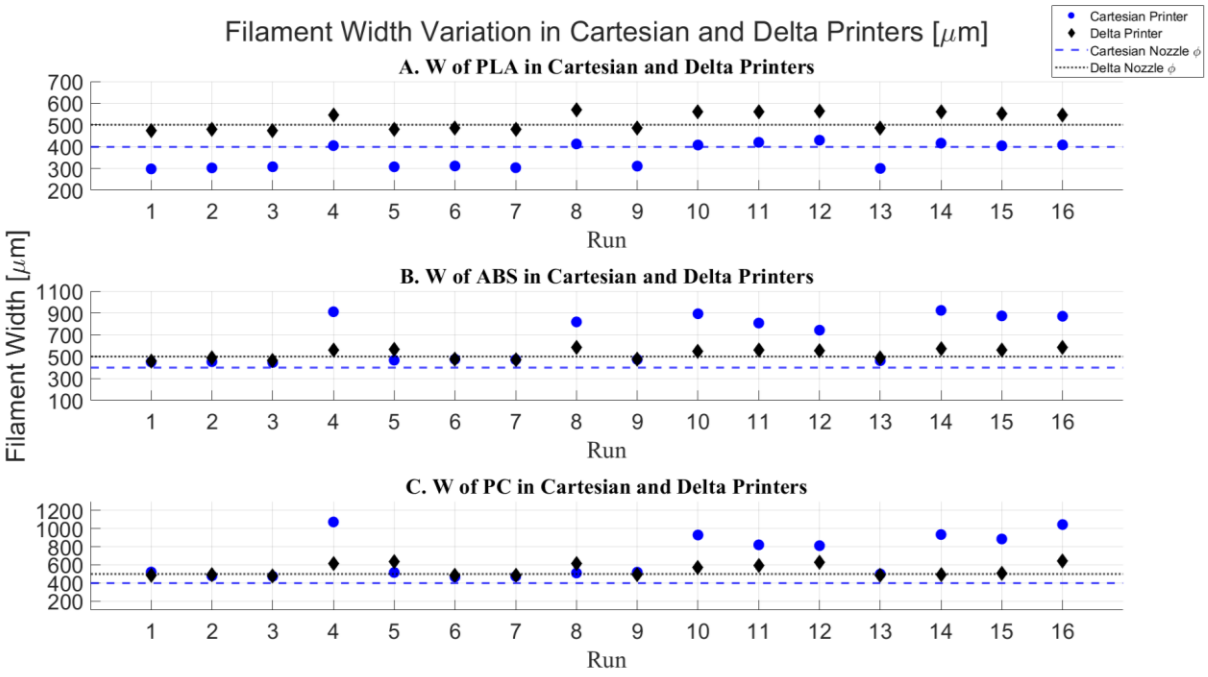

Figure 3. Filament width variation OM results of samples made in Delta printer and Cartesian printers with A. PLA, B. ABS, and C. PC.

PLA results

Samples of PLA made in a Cartesian printer showed a range in W of $131.96\mu m$ and an overall average in W of $359.13\mu m$ as seen in Figure 3A as blue dots. The model, Equation (1), for PLA in Cartesian printer considers LH, LH-ET, LH-FR,FR-BT because they have the greatest impact on filament width response, obtaining a $R^2 = 96.89\%$, and the residuals accomplished normality, homoscedasticity and independency, as shown in Figure 4A.

$$W_{PLA_{Cartesian}} = 359.13 - 53.93\,LH + 3.29\,ET * LH - 3.25\,FR * LH + 3.09\,FR * BT \quad \textbf{(1)}$$

Samples of PLA made in Delta printer showed a range in W of $96.73\ \mu m$ and an overall average in W of $519.33\ \mu m$, as seen in Figure 3A as black diamonds. The model for PLA in Delta printer, Equation (2), considers LH, FR, and LH-FR because they have the greatest impact on filament width response, obtaining a $R^2 = 94.61\%$, and residuals accomplished normality, homoscedasticity and independency, as shown in Figure 4B.

$$W_{PLA_{Delta}} = 519.33 - 38.39LH - 4.46\,LH * FR \quad \textbf{(2)}$$

A. PLA Delta residual analysis

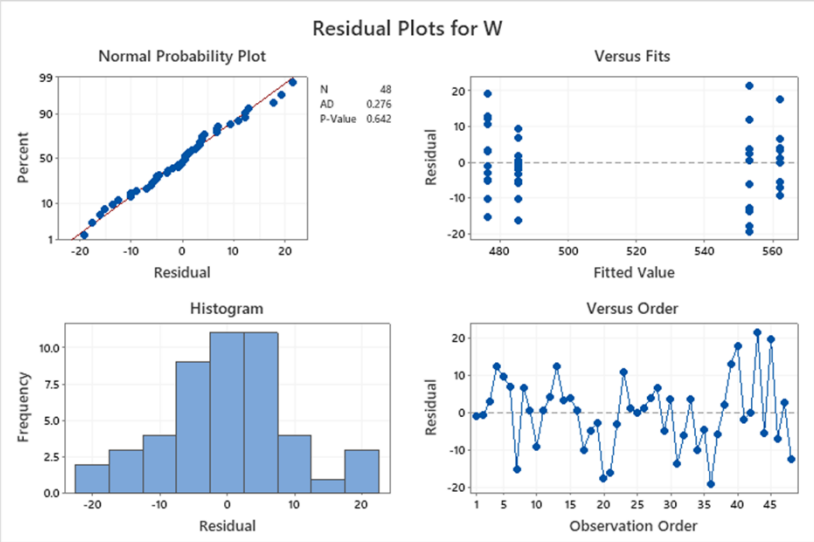

B. PLA Cartesian residual analysis

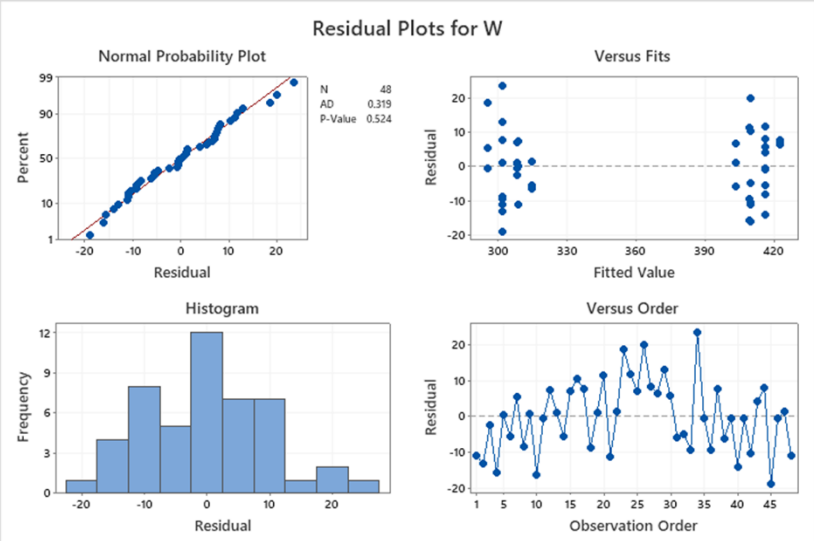

Figure 4. Residual analyses of W results of PLA samples made in A. Delta printer and B. Cartesian printer.

ABS results

Samples of ABS made in a Cartesian printer showed a range in W of $475\mu m$ and an overall average in W of $659.7\mu m$ as seen in Figure 3B as blue dots. The model for ABS in Cartesian printer, equation (3), considers LH, BT, ET-F, and FR-BT because they have the greatest impact on filament width response, obtaining a $R^2 = 95.54\%$, and the residuals accomplished normality, homoscedasticity, and independency, as shown in Figure 5A.

$$W_{ABS_{Cartesian}} = 659.66 - 195.45\ LH - 17.12\ BT + 18.41\ ET * F - 16.55\ FR * BT \quad \textbf{(1)}$$

Samples of ABS made in Delta printer showed a range of $124.14\mu m$ and an overall average of $520.65\mu m$ as seen in Figure 3B as black diamonds. The model for ABS in Delta printer, Equation (4), considers LH, F, BT and F-BT because they have the greatest impact on filament

width response, obtaining a $R^2 = 81.77\%$, and residuals accomplished normality, homoscedasticity, and independency, as shown in Figure 5B.

$$W_{ABS_{Delta}} = 672.6 - 893.9\ LH + 69.4\ F + 1.161\ BT - 1.223F * BT \quad \textbf{(2)}$$

A. ABS Delta residual analysis

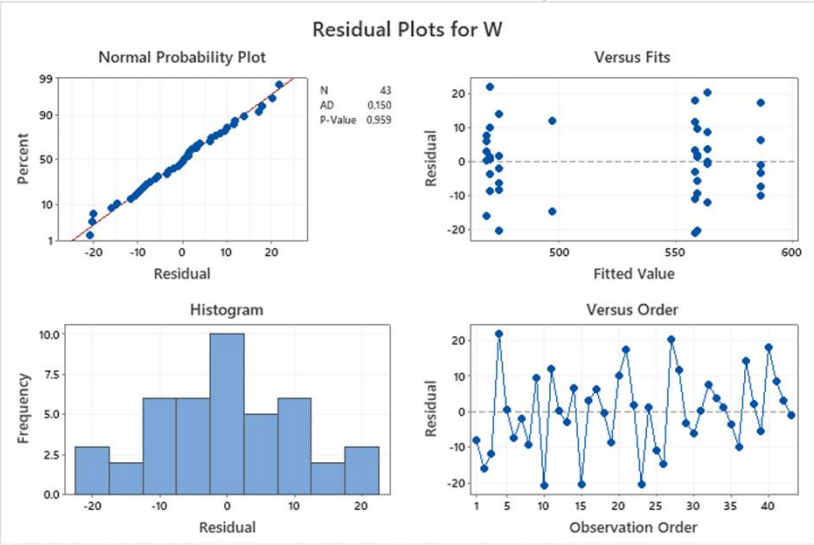

B. ABS Cartesian residual analysis

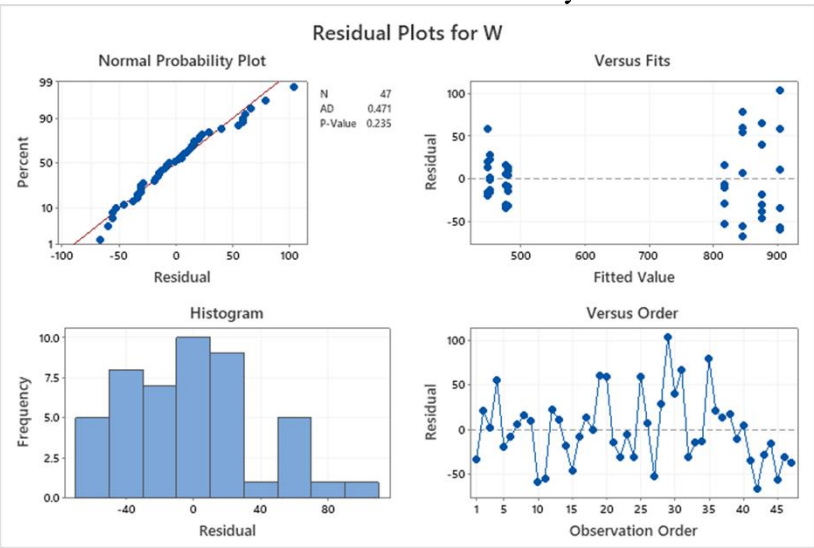

Figure 5 Residual analyses of W results of ABS samples made in A. Delta printer and B. Cartesian printer.

PC results

Samples of PC made in Cartesian printer showed a range of 606.11 μm and an overall average of 684.5 μm as seen in Figure 3C as blue dots. When the factorial analysis was done, the residual analysis states that the residuals do not have normal behavior. An outlier test was performed, and a single outlier was deleted from the data, then the residual analysis of the factorial

regression accomplishes normality, homoscedasticity, and independence. The model for PC in the Cartesian printer, equation (5), considers LH, FR, FR-F, FR-LH and FR-BT because they have the greatest impact on filament width response, obtaining a $R^2 = 84.2\%$, and residuals accomplished normality, homoscedasticity and independency, as shown in Figure 6E.

$$W_{PC_{Cartesian}} = 684.5 - 40.9\,FR - 191.5\,LH + 39\,FR * LH + 45.2\,FR * F - 38\,FR * BT \quad \textbf{(3)}$$

A. PC Delta residual analysis

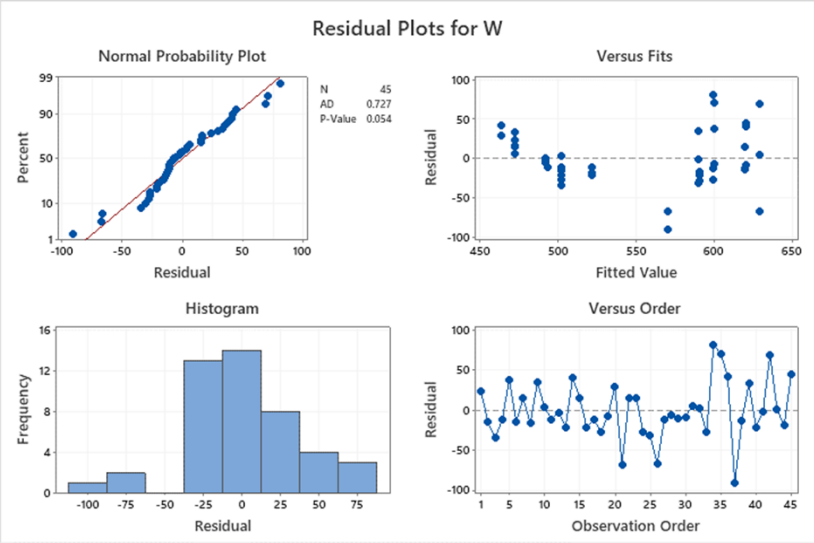

B. PC Cartesian residual analysis

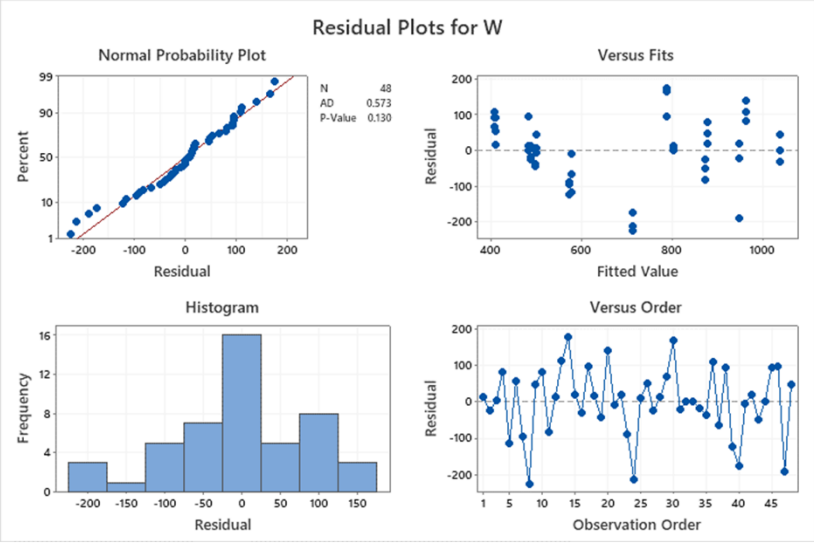

Figure 6 Residual analyses of W results of PC samples made in A. Delta printer and B. Cartesian printer.

Samples of PC made in Delta printer showed a range of 155.88 μm and an overall average of 543.6 μm as seen in Figure 3C as black diamonds. The model for PC in Delta printer equation (6), considers LH, BT, FR-F, ET-F, and F-BT because they have the greatest impact on filament width response, obtaining a $R^2 = 72.74\%$, and residuals accomplished normality, homoscedasticity and independency, as shown in Figure 6F.

$$W_{PC_{Delta}} = 546.17 - 36.7\,LH + 14.85\,BT - 26.62\,ET * F + 28.81\,FR * F - 22.24\,F * BT \quad \textbf{(4)}$$

Response optimization

When regression models were obtained, they were summited to a response optimization. The optimization was specified to find the value of W closest to the diameter of the extruder used in each printer, 400 μm for the Cartesian printer and 500 μm for the Delta printer. Table 4 shows the results of the different printing parameters that were fitted on the response optimization process.

Table 4. Printing parameter values approximating the predicted W to the diameter of the extruder used in each printer.

Printer	*Material*	*ET* $[°C]$	*FR* $[mm^3/s]$	*LH* $[mm]$	*F*	*BT* $[°C]$	*W prediction* $[\mu m]$
Delta	PLA	-	720	0.3	-	-	556.89
	ABS	-	-	0.3	0	80	517.7
	PC	250	720	0.3	1	80	501.88
Cartesian	PLA	215	1800	0.1	-	60	416.17
	ABS	230	1800	0.2	1	80	421.17
	PC	-	1800	0.2	0	80	407.8

In Delta printer, LH is the only parameter that is included in the regression models for PLA, ABS and PC. In Cartesian printers LH, FR and BT are included either as individual effect or as parameter interactions. All the regression analysis showed that LH has the largest impact on W, the lower LH, the higher W, as showed in Figure 7. As in Nuñez et al.[54], the higher LH selected gave the most accurate dimensional behavior.

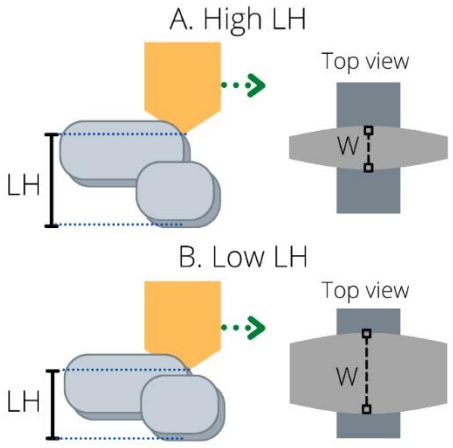

Figure 7. LH effect on extruded filament width. A. High LH decreases the W and B. Low LH increases the W.

When the printers are compared, the Cartesian printer results showed higher standard deviations in W of ABS and PC, 206.7 and 229.4, respectively, in comparison with the Delta printer standard deviations, 49.10 and 69.8, for ABS and PC, respectively. Meaning that the dispersion of extruded filament width of ABS and PC is closer to the nozzle diameter in Delta printer than in Cartesian printer.

The Cartesian printer regression models have in common LH, BT, and FR as the printing parameters that most affect W. The regression models obtained for the Delta printer have in common LH as the printing parameter that affects W in all the thermoplastics used.

Conclusions

A fractional factorial design of experiments was used to find the effects of the parameters ET, LH, BT, F, and FR on filament width (W). It also helped to find predictive models for extruded filament width, using the least number of parameters and interactions between them, as well as the values of these parameters to have filaments with a thickness similar to the size of the extruder of the printers and thus obtain a homogeneous structure that has the same properties throughout the piece. Not having irregularities or variations will help to have a structure without stress concentrators that affect the result of any mechanical property at the time of performing mechanical tests on products made by FFF.

The effect of layer height needs to be further analyzed to improve the control of FFF product dimensions. It is necessary to analyze the layer height at different levels to reach a higher control of extruded filament width. With the control of the filament width, the internal structures of FFF parts can be controlled, reaching higher physical and mechanical properties on these parts.

Acknowledgment

We thank Metamaterials Lab and Mechanical Lab of Tecnologico de Monterrey, Campus Queretaro for the support given to this research.

Funding Information

This work was supported by Tecnologico de Monterrey with an academic scholarship (Grant No. A01206366) and by Consejo Nacional de Ciencia y Tecnología (CONACyT) with an economic grant (Grant No. 1045844).

References

1. Chohan, J.S.; Singh, R. Pre and Post Processing Techniques to Improve Surface Characteristics of FDM Parts: A State of Art Review and Future Applications. *Rapid Prototyp J* **2017**, *23*, 495–513, doi:10.1108/RPJ-05-2015-0059.
2. Khorram Niaki, M.; Nonino, F.; Palombi, G.; Torabi, S.A. Economic Sustainability of Additive Manufacturing: Contextual Factors Driving Its Performance in Rapid Prototyping. *Journal of Manufacturing Technology Management* **2019**, *30*, 353–365, doi:10.1108/JMTM-05-2018-0131.
3. Mahmood, S.; Qureshi, A.J.; Goh, K.L.; Talamona, D. Tensile Strength of Partially Filled FFF Printed Parts: Experimental Results. *Rapid Prototyp J* **2017**, *23*, 122–128, doi:10.1108/RPJ-08-2015-0115.
4. Jin, Y.; He, Y.; Fu, G.; Zhang, A.; Du, J. A Non-Retraction Path Planning Approach for Extrusion-Based Additive Manufacturing. *Robot Comput Integr Manuf* **2017**, *48*, 132–144, doi:10.1016/j.rcim.2017.03.008.

5. Kumar, A.; Verma, S.; Jeng, J.Y. Supportless Lattice Structures for Energy Absorption Fabricated by Fused Deposition Modeling. *3D Print Addit Manuf* **2020**, *7*, 85–96, doi:10.1089/3dp.2019.0089.

6. Hsieh, C.T. Investigation of Delta Robot 3D Printer for a Good Quality of Printing. *Applied Mechanics and Materials* **2017**, *870*, 164–169, doi:10.4028/www.scientific.net/amm.870.164.

7. Oo, H.L.; Ye, K.Z.; Linn, Y.H. Modeling and Controlling of Temperature in 3D Printer (FDM). *Proceedings of the 2018 IEEE Conference of Russian Young Researchers in Electrical and Electronic Engineering, ElConRus 2018* **2018**, *18*, 1738–1742, doi:10.1109/EIConRus.2018.8317441.

8. Tymrak, B.M.; Kreiger, M.; Pearce, J.M. Mechanical Properties of Components Fabricated with Open-Source 3D Printers Under Realistic Environmental Conditions. *Mater Des* **2014**, *58*, 242–246, doi:10.1016/j.matdes.2014.02.038.

9. Taylor, A.P.; García, L.F.V. High-Temperature Compatible, Monolithic, 3D-Printed Magnetic Actuators. **2018**.

10. Gordeev, E.G.; Galushko, A.S.; Ananikov, V.P. Improvement of Quality of 3D Printed Objects by Elimination of Microscopic Structural Defects in Fused Deposition Modeling. *PLoS One* **2018**, *13*, doi:10.1371/journal.pone.0198370.

11. Fayazbakhsh, K.; Movahedi, M.; Kalman, J. The Impact of Defects on Tensile Properties of 3D Printed Parts Manufactured by Fused Filament Fabrication. *Mater Today Commun* **2019**, *18*, 140–148, doi:10.1016/j.mtcomm.2018.12.003.

12. Weeren, R. van; Agarwala, M.; Jamalabad, V.R.; Bandyophadyay, A.; Vaidyanathan, R.; Langrana, N.; Safari, A.; Whalen, P.; Danforth, S.C.; Ballard, C. Quality of Parts Processed by Fused Deposition. *Solid Freeform Fabrication* **1995**, 314–321.

13. Rodríguez-Panes, A.; Claver, J.; Camacho, A.M. The Influence of Manufacturing Parameters on the Mechanical Behaviour of PLA and ABS Pieces Manufactured by FDM: A Comparative Analysis. *Materials* **2018**, *11*, doi:10.3390/ma11081333.

14. ben Ali, N.; Khlif, M.; Hammami, D.; Bradai, C. Mechanical and Morphological Characterization of Spherical Cell Porous Structures Manufactured Using FDM Process. *Eng Fract Mech* **2019**, *216*, doi:10.1016/j.engfracmech.2019.106527.

15. Cuiffo, M.A.; Snyder, J.; Elliott, A.M.; Romero, N.; Kannan, S.; Halada, G.P. Impact of the Fused Deposition (FDM) Printing Process on Polylactic Acid (PLA) Chemistry and Structure. *Applied Sciences (Switzerland)* **2017**, *7*, 1–14, doi:10.3390/app7060579.

16. Wickramasinghe, S.; Do, T.; Tran, P. FDM-Based 3D Printing of Polymer and Associated Composite: A Review on Mechanical Properties, Defects and Treatments. *Polymers (Basel)* **2020**, *12*, 1–42, doi:10.3390/polym12071529.

17. Choi, Y.-H.; Kim, C.-M.; Jeong, H.-S.; Youn, J.-H. Influence of Bed Temperature on Heat Shrinkage Shape Error in FDM Additive Manufacturing of the ABS-Engineering Plastic. *World Journal of Engineering and Technology* **2016**, *04*, 186–192, doi:10.4236/wjet.2016.43d022.

18. Azdast, T.; Hasanzadeh, R. Polylactide Scaffold Fabrication Using a Novel Combination Technique of Fused Deposition Modeling and Batch Foaming: Dimensional Accuracy and Structural Properties. *The International Journal of Advanced Manufacturing Technology* **2021**, *114*, 1309–1321, doi:10.1007/s00170-021-06915-9.

19. Ertay, D.S.; Yuen, A.; Altintas, Y. Synchronized Material Deposition Rate Control with Path Velocity on Fused Filament Fabrication Machines. *Addit Manuf* **2018**, *19*, 205–213, doi:10.1016/j.addma.2017.05.011.

20. Santana, L.; Lino Alves, J.; da Costa Sabino Netto, A. A Study of Parametric Calibration for Low Cost 3D Printing: Seeking Improvement in Dimensional Quality. *Mater Des* **2017**, *135*, 159–172, doi:10.1016/j.matdes.2017.09.020.

21. Geng, P.; Zhao, J.; Wu, W.; Ye, W.; Wang, Y.; Wang, S.; Zhang, S. Effects of Extrusion Speed and Printing Speed on the 3D Printing Stability of Extruded PEEK Filament. *J Manuf Process* **2019**, *37*, 266–273, doi:10.1016/j.jmapro.2018.11.023.

22. García Plaza, E.; Núñez López, P.; Caminero Torija, M.; Chacón Muñoz, J. Analysis of PLA Geometric Properties Processed by FFF Additive Manufacturing: Effects of Process Parameters and Plate-Extruder Precision Motion. *Polymers (Basel)* **2019**, *11*, 1581, doi:10.3390/polym11101581.

23. Liu, J.; Gaynor, A.T.; Chen, S.; Kang, Z.; Suresh, K.; Takezawa, A.; Li, L.; Kato, J.; Tang, J.; Wang, C.C.L.; et al. Current and Future Trends in Topology Optimization for Additive Manufacturing. *Structural and Multidisciplinary Optimization* **2018**, *57*, 2457–2483, doi:10.1007/s00158-018-1994-3.

24. Calignano, F.; Lorusso, M.; Roppolo, I.; Minetola, P. Investigation of the Mechanical Properties of a Carbon Fibre-Reinforced Nylon Filament for 3d Printing. *Machines* **2020**, *8*, 1–13, doi:https://doi.org/10.3390/machines8030052.

25. Medellin-Castillo, H.I.; Zaragoza-Siqueiros, J. Design and Manufacturing Strategies for Fused Deposition Modelling in Additive Manufacturing: A Review. *Chinese Journal of Mechanical Engineering* **2019**, *32*, 53, doi:10.1186/s10033-019-0368-0.

26. Xia, H.; Lu, J.; Dabiri, S.; Tryggvason, G. Fully Resolved Numerical Simulations of Fused Deposition Modeling. Part I: Fluid Flow. *Rapid Prototyp J* **2018**, *24*, 463–476, doi:10.1108/RPJ-12-2016-0217.

27. Xia, H.; Lu, J.; Tryggvason, G. A Numerical Study of the Effect of Viscoelastic Stresses in Fused Filament Fabrication. *Comput Methods Appl Mech Eng* **2019**, *346*, 242–259, doi:10.1016/j.cma.2018.11.031.

28. Vyavahare, S.; Kumar, S.; Panghal, D. Experimental Study of Surface Roughness, Dimensional Accuracy and Time of Fabrication of Parts Produced by Fused Deposition Modelling. *Rapid Prototyp J* **2020**, *26*, 1535–1554, doi:10.1108/RPJ-12-2019-0315.

29. Mohamed, O.A.; Masood, S.H.; Bhowmik, J.L. Experimental Investigations of Process Parameters Influence on Rheological Behavior and Dynamic Mechanical Properties of FDM Manufactured Parts. *Materials and Manufacturing Processes* **2016**, *31*, 1983–1994, doi:10.1080/10426914.2015.1127955.

30. Fountas, N.A.; Papantoniou, I.; Kechagias, J.D.; Manolakos, D.E.; Vaxevanidis, N.M. Modeling and Optimization of Flexural Properties of FDM-Processed PET-G Specimens Using RSM and GWO Algorithm. *Eng Fail Anal* **2022**, *138*, 1350–1362, doi:10.1016/j.engfailanal.2022.106340.

31. Sood, A.K.; Equbal, A.; Toppo, V.; Ohdar, R.K.; Mahapatra, S.S. An Investigation on Sliding Wear of FDM Built Parts. *CIRP J Manuf Sci Technol* **2012**, *5*, 48–54, doi:10.1016/j.cirpj.2011.08.003.

32. Pazhamannil, R.V.; Govindan, P.; Sooraj, P. Prediction of the Tensile Strength of Polylactic Acid Fused Deposition Models Using Artificial Neural Network Technique. *Mater Today Proc* **2020**, 1–7, doi:10.1016/j.matpr.2020.01.199.

33. Ansari, A.A.; Kamil, M. Performance Study of 3D Printed Continuous Fiber-Reinforced Polymer Composites Using Taguchi Method. *J Mater Eng Perform* **2022**, doi:10.1007/s11665-022-07715-2.

34. Lanzotti, A.; Grasso, M.; Staiano, G.; Martorelli, M. The Impact of Process Parameters on Mechanical Properties of Parts Fabricated in PLA Ith an Open-Source 3D Printer. *Rapid Prototyp J* **2015**, *21*, 604–617, doi:10.1108/RPJ-09-2014-0135.

35. Sood, A.K.; Ohdar, R.K.; Mahapatra, S.S. Experimental Investigation and Empirical Modelling of FDM Process for Compressive Strength Improvement. *J Adv Res* **2012**, *3*, 81–90, doi:10.1016/J.JARE.2011.05.001.

36. Mohamed, O.A.; Masood, S.H.; Bhowmik, J.L. Experimental Investigation of the Influence of Fabrication Conditions on Dynamic Viscoelastic Properties of PC-ABS Processed Parts by FDM Process. *IOP Conf Ser Mater Sci Eng* **2016**, *149*, doi:10.1088/1757-899X/149/1/012122.

37. Torres, J.; Cotelo, J.; Karl, J.; Gordon, A.P. Mechanical Property Optimization of FDM PLA in Shear with Multiple Objectives. *JOM* **2015**, *67*, 1183–1193, doi:10.1007/s11837-015-1367-y.

38. Ziemian, C.; Sharma, M.; Ziemi, S. Anisotropic Mechanical Properties of ABS Parts Fabricated by Fused Deposition Modelling. *Mechanical Engineering* **2012**, doi:10.5772/34233.

39. Mohamed, O.A.; Masood, S.H.; Bhowmik, J.L.; Nikzad, M.; Azadmanjiri, J. Effect of Process Parameters on Dynamic Mechanical Performance of FDM PC/ABS Printed Parts Through Design of Experiment. *J Mater Eng Perform* **2016**, *25*, 2922–2935, doi:10.1007/s11665-016-2157-6.

40. Zhang, J.; Wang, P.; Gao, R.X. Deep Learning-Based Tensile Strength Prediction in Fused Deposition Modeling. *Comput Ind* **2019**, *107*, 11–21, doi:10.1016/j.compind.2019.01.011.

41. Hooda, N.; Singh Chohan, J.; Gupta, R.; Kumar, R. Deposition Angle Prediction of Fused Deposition Modeling Process Using Ensemble Machine Learning. *ISA Trans* **2021**, *116*, 121–128, doi:10.1016/j.isatra.2021.01.035.

42. Kumar, S.; Bhushan, P.; Sinha, N.; Prakash, O.; Bhattacharya, S. Investigation of Structure–Mechanical Property Relationship in Fused Filament Fabrication of the Polymer

Composites. *Journal of Micromanufacturing* **2019**, *2*, 167–174, doi:10.1177/2516598419843687.

43. Mohamed, O.A.; Masood, S.H.; Bhowmik, J.L. Experimental Investigation of Creep Deformation of Part Processed by Fused Deposition Modeling Using Definitive Screening Design. *Addit Manuf* **2017**, *18*, 164–170, doi:10.1016/j.addma.2017.10.013.

44. Zeng, C.; Liu, L.; Bian, W.; Liu, Y.; Leng, J. 4D Printed Electro-Induced Continuous Carbon Fiber Reinforced Shape Memory Polymer Composites with Excellent Bending Resistance. *Compos B Eng* **2020**, *194*, 108034, doi:10.1016/j.compositesb.2020.108034.

45. Moretti, M.; Senin, N. In-Process Monitoring of Part Warpage in Fused Filament Fabrication through the Analysis of the Repulsive Force Acting on the Extruder. *Addit Manuf* **2022**, *49*, 102505, doi:10.1016/j.addma.2021.102505.

46. Armillotta, A.; Bellotti, M.; Cavallaro, M. Warpage of FDM Parts: Experimental Tests and Analytic Model. *Robot Comput Integr Manuf* **2018**, *50*, 140–152, doi:10.1016/j.rcim.2017.09.007.

47. Barrios; Romero Decision Tree Methods for Predicting Surface Roughness in Fused Deposition Modeling Parts. *Materials* **2019**, *12*, 2574, doi:10.3390/ma12162574.

48. Liu, J.; Ye, J.; Momin, F.; Zhang, X.; Li, A. Nonparametric Bayesian Framework for Material and Process Optimization with Nanocomposite Fused Filament Fabrication. *Addit Manuf* **2022**, *54*, 2214–8604, doi:10.1016/j.addma.2022.102765.

49. Gleadall, A.; Ashcroft, I.; Segal, J. VOLCO: A Predictive Model for 3D Printed Microarchitecture. *Addit Manuf* **2018**, *21*, 605–618, doi:10.1016/j.addma.2018.04.004.

50. Hebda, M.; McIlroy, C.; Whiteside, B.; Caton-Rose, F.; Coates, P. A Method for Predicting Geometric Characteristics of Polymer Deposition During Fused-Filament-Fabrication. *Addit Manuf* **2019**, *27*, 99–108, doi:10.1016/j.addma.2019.02.013.

51. Yousefi, A.M.; Smucker, B.; Naber, A.; Wyrick, C.; Shaw, C.; Bennett, K.; Szekely, S.; Focke, C.; Wood, K.A. Controlling the Extrudate Swell in Melt Extrusion Additive Manufacturing of 3D Scaffolds: A Designed Experiment. *J Biomater Sci Polym Ed* **2018**, *29*, 195–216, doi:10.1080/09205063.2017.1409022.

52. Shahriar, B.B.; France, C.; Valerie, N.; Arthur, C.; Christian, G. Toward Improvement of the Properties of Parts Manufactured by FFF (Fused Filament Fabrication) through Understanding the Influence of Temperature and Rheological Behaviour on the Coalescence Phenomenon. In Proceedings of the AIP Conference Proceedings; 2017; Vol. 1896, p. 040008.

53. Valerga, A.P.; Batista, M.; Salguero, J.; Girot, F. Influence of PLA Filament Conditions on Characteristics of FDM Parts. *Materials* **2018**, *11*, doi:10.3390/ma11081322.

54. Nuñez, P.J.; Rivas, A.; García-Plaza, E.; Beamud, E.; Sanz-Lobera, A. Dimensional and Surface Texture Characterization in Fused Deposition Modelling (FDM) with ABS Plus. *Procedia Eng* **2015**, *132*, 856–863, doi:10.1016/j.proeng.2015.12.570.